



**HAL**  
open science

## Shock front nonstationarity and ion acceleration in supercritical perpendicular shocks

Z.W. Yang, Q.M. Lu, Bertrand Lembège, S. Wang

► **To cite this version:**

Z.W. Yang, Q.M. Lu, Bertrand Lembège, S. Wang. Shock front nonstationarity and ion acceleration in supercritical perpendicular shocks. *Journal of Geophysical Research Space Physics*, 2009, 114 (A3), pp.A03111. 10.1029/2008JA013785 . hal-00372232

**HAL Id: hal-00372232**

**<https://hal.science/hal-00372232>**

Submitted on 12 Mar 2016

**HAL** is a multi-disciplinary open access archive for the deposit and dissemination of scientific research documents, whether they are published or not. The documents may come from teaching and research institutions in France or abroad, or from public or private research centers.

L'archive ouverte pluridisciplinaire **HAL**, est destinée au dépôt et à la diffusion de documents scientifiques de niveau recherche, publiés ou non, émanant des établissements d'enseignement et de recherche français ou étrangers, des laboratoires publics ou privés.

## Shock front nonstationarity and ion acceleration in supercritical perpendicular shocks

Z. W. Yang,<sup>1</sup> Q. M. Lu,<sup>1</sup> B. Lembège,<sup>2</sup> and S. Wang<sup>1</sup>

Received 30 September 2008; revised 9 December 2008; accepted 14 January 2009; published 31 March 2009.

[1] Previous particle-in-cell simulations have evidenced that quasiperpendicular shocks are nonstationary and suffer a self-reformation on gyro scale of the incoming ions due to the accumulation of reflected ions. In this paper, by separating the incoming ions into reflected and directly transmitted parts, we investigate the detailed mechanisms of ion acceleration in a nonstationary perpendicular shock. Test particle simulations are performed where the shock profiles are issued from self-consistent one-dimensional full particle-in-cell simulations. Both shell and Maxwellian incoming ion distributions are used. In both cases, most energetic particles correspond to reflected ions, and the associated acceleration mechanisms include both shock drift acceleration (SDA) and shock surfing acceleration (SSA). Two types of results are obtained. First, if we fix the shock profiles at different times within a self-reformation cycle, the mechanisms of particle acceleration are different at different profiles. SDA process appears as the dominant acceleration mechanism when the width of the ramp is broad (and overshoot amplitude is low) whereas both SDA and SSA contribute as the width of the ramp is narrow (and overshoot amplitude is high). For the different shock profiles concerned herein, SDA process is more efficient (higher resulting ion energy gain) than the SSA process. Second, in order to investigate ion acceleration in self-reforming shocks, not only the ramp but also the variations of the whole shock front need to be included. In the continuously time-evolving shock, SDA remains a dominant acceleration mechanism whereas SSA mechanism becomes more and more important with the increase of the initial particle energy. The percentage of reflected ions cyclically varies in time with a period equal to the self reformation cycle, which is in agreement with previous full particle simulations. The reflected ions not only come from the distribution wings of the incoming ions but also from the core part, in contrast with previous results based on stationary shocks.

**Citation:** Yang, Z. W., Q. M. Lu, B. Lembège, and S. Wang (2009), Shock front nonstationarity and ion acceleration in supercritical perpendicular shocks, *J. Geophys. Res.*, *114*, A03111, doi:10.1029/2008JA013785.

### 1. Introduction

[2] Collisionless shocks are of fundamental interests in space physics, plasma physics and astrophysics. They are commonly believed to be important sources for high-energy particles, such as those observed at planetary shocks (as at terrestrial bow shock), anomalous cosmic rays (ACRs) or solar energetic particles (SEPs). At quasiparallel shocks, the theory of diffusive shock acceleration (DSA) is quite successful to account for observed energetic particles [Axford *et al.*, 1977; Bell, 1978a, 1978b; Blandford and Ostriker, 1978; Lee, 1983; Blandford and Eichler, 1987; Webb *et al.*, 1995; Malkov and Drury, 2001; Li *et al.*, 2003;

Giacalone, 2004; Zank *et al.*, 2006]. The upstream ions reflected by quasiparallel shocks can go far upstream along the magnetic field line, and can excite low-frequency plasma waves which in turn scatter the ions interacting with the shock front many times. In this way, the ions can be accelerated to high energy. However, a similar theory does not work at quasiperpendicular shocks, where the reflected upstream ions return to the shocks almost immediately due to the gyromotion in the magnetic field. Therefore, the quasiperpendicular shocks cannot provide self-produced plasma waves with large spatial/temporal scales similar to ULF waves observed at quasiparallel waves [Tsubouchi and Lembège, 2004] to scatter the particles.

[3] Shock drift acceleration (SDA) [Hudson, 1965; Webb *et al.*, 1983; Decker, 1988] and shock surfing acceleration (SSA) [Sagdeev, 1966; Katsouleas and Dawson, 1983; Lipatov *et al.*, 1998; Ucer and Shapiro, 2001, 2005] are considered to play important roles in ion acceleration at quasiperpendicular shocks. In shock drift acceleration, the particles gain energy as their guiding centers move along

<sup>1</sup>School of Earth and Space Sciences, University of Science and Technology of China, Hefei, China.

<sup>2</sup>Centre d'étude des Environnements Terrestre et Planétaires, CNRS Université de Versailles-Saint Quentin, Velizy, France.

**Table 1.** Upstream Plasma Parameters Defined for PIC Simulations

		Electrons	Ions
Thermal velocity	$\tilde{V}_{thx,y,z}$	0.2	0.017
Debye length	$\lambda_D$	0.2	0.16
Larmor gyroradius	$\tilde{\rho}_e$	0.4	2.91
Inertia length	$\tilde{c}/\tilde{\omega}_p$	3.0	27.5
Gyro frequency	$\tilde{\Omega}_c$	0.5	0.006
Plasma frequency	$\tilde{\omega}_p$	1.0	0.11
Gyro period	$\tilde{\tau}_c$	12.55	1055.46
Plasma beta	$\tilde{\beta}$	0.0355	0.0225

the convective electric field due to the drift effects of the magnetic field gradient or the curvature of the shock front [Decker and Vlahos, 1985; Begelman and Kirk, 1990; Chalov, 2001]. In shock surfing acceleration, the particles are reflected by the shock potential, and then they return to the shock front due to the upstream Lorentz force. In this process, these particles are trapped at the shock front and accelerated by the convective electric field. They may repeat the process several times until they have acquired sufficient kinetic energy to overcome the macroscopic potential barrier at the shock front [Zank et al., 1996; Lee et al., 1996; Lee, 1999; Shapiro and Ucer, 2003]. With hybrid simulations, Burgess et al. [1989] have analyzed ion acceleration at quasiperpendicular shocks by separating the incoming ions into directly transmitted and reflected parts. They found that none of the reflected ions comes from the core of the upstream velocity distribution, and those reflected ions form the high energy tail of the downstream distribution. Lipatov and Zank [1999] investigated shock surfing acceleration of pickup ions at perpendicular shocks, and found that the width of shock ramp is the key factor determining the efficiency of shock surfing acceleration. Lever et al. [2001] compared the efficiency of shock surfing and shock drift acceleration mechanisms for different widths of shock ramp, and they demonstrated that SSA process predominates when the width of shock ramp is below a critical value. However, the used ramp width was not obtained self-consistently, which has strong consequences as shown in the present study.

[4] In the above studies, the structures of quasiperpendicular shocks are based on hybrid simulations, the used spatial resolution (and the minimum width of the shock ramp) is roughly  $\sim 0.5 - 1c/\omega_{pi}$  (where  $c/\omega_{pi}$  is the ion inertial length). As a consequence, the shock profile is stationary as the spatial resolution is not high enough to allow the self-reformation to set up [Hellinger et al., 2002].

[5] On the other side, particle-in-cell simulations clearly evidence that quasiperpendicular supercritical shocks are nonstationary and suffer a self-reformation on the gyro scale of the incoming proton due to the accumulation of reflected ions (foot formation) [Biskamp and Welter, 1972; Lembege and Dawson, 1987; Lembege and Savoini, 1992; Shimada and Hoshino, 2000; Schmitz et al., 2002; Scholer et al., 2003; Nishimura et al., 2003]. More precisely, the cyclic period of this process is of the order of ion gyroperiod calculated from the average magnetic field measured in the middle of the ramp as measured by Lembege and Savoini [1992]. During the self-reformation of the shock front, the ramp width can vary largely and reaches a very narrow value  $\sim 4 - 5 c/\omega_{pe}$  (where  $c/\omega_{pe}$  is the electron inertial

length). This self-reformation is observed for a certain range of parameters (high values of the Alfvén Mach number and/or low beta-i) as shown by Hellinger et al. [2002] and Hada et al. [2003], and persists quite well even for realistic mass ratio [Scholer and Matsukiyo, 2004].

[6] Lee et al. [2004, 2005] further studied ion accelerations at nonstationary perpendicular shocks with PIC simulations. They found that the efficiency of the ions accelerated to high energy depends on the time at which they arrive at the shock. In this paper, by separating ions into directly transmitted and reflected parts, we investigate the ion acceleration mechanisms with different initial energy in the nonstationary perpendicular shock obtained from one-dimensional PIC simulations.

[7] The paper is organized as follows. In section 2, we briefly describe the simulation model. The results from our test particle simulations are presented in section 3. The discussion and conclusions are summarized in section 4.

## 2. Simulation Model

[8] In this paper, self-consistent perpendicular shock profiles are obtained from one-dimensional PIC simulations. The initial and boundary conditions are similar to those already explained in detail by Lembege and Savoini [1992], and the shock is initiated by a magnetic piston (applied current pulse). Therefore, the shock geometry is defined in the upstream frame: the shock propagates along the  $x$  direction and an upstream magnetic field  $B_0$  is applied along the  $z$  direction. All dimensionless quantities are indicated by a tilde “ $\sim$ ” and are normalized as follows. The spatial coordinate is  $\tilde{x} = x/\Delta$ ; velocity  $\tilde{v} = v/\omega_{pe}\Delta$ ; time  $\tilde{t} = \omega_{pe}t$ , electric field  $\tilde{E} = eE/m_e\omega_{pe}^2\Delta$ ; magnetic field  $\tilde{B} = eB/m_e\omega_{pe}^2\Delta$ . The parameters  $\Delta$ ,  $\omega_{pe}$ ,  $m_e$  and  $e$  are, respectively, the numerical grid size, the electron plasma frequency, the electron mass and the electric charge. All basic parameters are identical to those used in Hada et al. [2003]: plasma box size length  $L_x = 4096$ ; velocity of light  $\tilde{c} = 3$ , and mass ratio  $m_i/m_e = 84$ . Initially, the particle density is  $n_e = n_i = 50$  at each grid point. With the decrease of electron/ion temperature ratio, the nonstationarity of the shock will be less obvious [Hada et al., 2003], and the electron/ion temperature ratio  $T_e/T_i = 1.58$  is chosen in order to investigate the particle acceleration at a reforming shock. The ambient magnetic field is  $|\tilde{B}_0| = 1.5$ . The shock front is propagating along  $x$  direction in a supercritical regime with the average Mach number about ( $M_A = 5.24$ ), where  $M_A = \tilde{V}_{shock}/\tilde{V}_A$  is determined in the upstream plasma (i.e. simulation) frame; the Alfvén velocity  $\tilde{V}_A$  is equal to 0.16. For these initial conditions, the plasma parameters are summarized in Table 1 for both electrons and ions. The Larmor gyroradius in Table 1 is calculated based on thermal velocity. However, in this paper we are interested in the acceleration of ions, which have higher energy than that corresponding to thermal velocity.

## 3. Simulation Results

[9] The time evolution of the perpendicular shock is shown in Figure 1, which plots the magnetic field  $\tilde{B}_z$  within the spatial range  $\tilde{X} = 4600$  to 5900. The shock is nonstationary, and a self-reforming shock front is observed. The red line in Figure 1 describes the ramp position of the shock

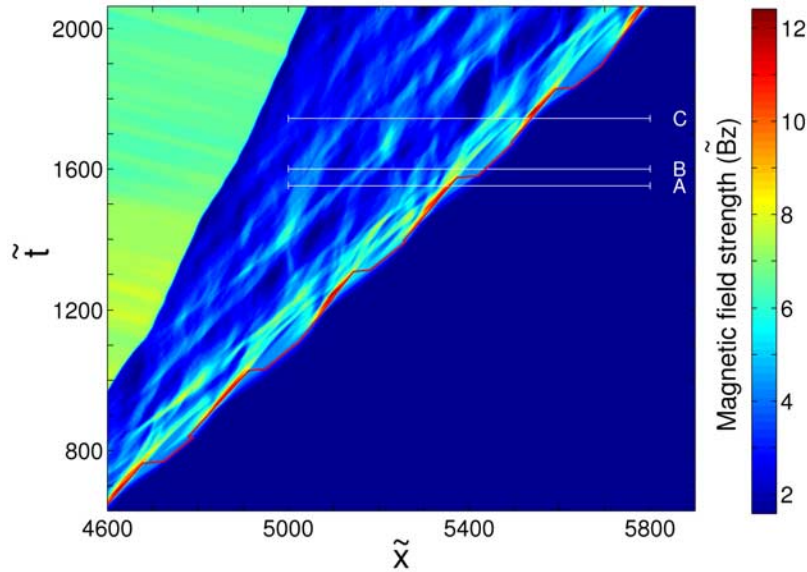


**Figure 1.** The time evolution of  $\tilde{B}_z$  versus  $\tilde{X}$ . A, B, and C indicate the shock profiles that are chosen in Figure 2 within one cyclic self-reformation of the shock front. The red line describes the position of the shock ramp.

ramp. The shock is in supercritical regime characterized by a noticeable density of reflected ions responsible for the formation of the foot located upstream of the ramp and for the overshoot. The ratio of downstream and upstream magnetic field is about 3.0, which is consistent with MHD jump condition [Burgess, 1995]. At  $\tilde{t} = 650$ , the shock front is at about  $\tilde{X} = 4600$ . Later at about  $\tilde{t} = 800$ , the reflected ions have accumulated in the foot with a percentage relatively high so that the foot amplitude increases and reaches a value comparable to that of the “old” ramp. Then, a “new” shock ramp builds up and starts reflecting new incoming ions. The “new” shock front is well formed around  $\tilde{X} = 4850$  at about  $\tilde{t} = 950$ . Simultaneously, the “old” shock front becomes weaker and weaker and is located downstream of the “new” front. The shock front is characterized by a self-reformation with a cyclic period about  $288\omega_{pe}^{-1} \approx 1.73\Omega_{ci}^{-1}$ .

[10] In this paper, we investigate in detail ion acceleration in this predefined nonstationary perpendicular shock with test particle simulations. We follow the trajectories of 12000 particles, which are released with different kinetic energy. For a given time, a shock profile is selected and interacts with test ions during its propagation. For all test particle simulations performed herein, the incoming ions are distributed evenly in the region  $100 < \tilde{x}_i - \tilde{x}_{\text{ramp}} < 1420$ , where  $\tilde{x}_i$  is the position of ions, and  $\tilde{x}_{\text{ramp}}$  is the position of the shock ramp, which is determined by  $|\partial\tilde{B}_z^2/\partial\tilde{x}|_{\text{max}}$  (inflection point in the ramp of  $B_z$  profile). In the simulation, the width of the upstream region filled with test particles is sufficiently large, and it takes about 5 shock reforming cycles to advect these particles through the shock. If no explicitly mentioned, the distribution of the test particle velocities is initially described as shell function, and ions only differ by their phase angles on the shell. All particles have same kinetic energy, and the shell radius defines the kinetic energy of the particles. Here, the propagating shock is injected with a velocity equal to that measured in the PIC

simulations; its instantaneous Mach number can differ from the average value ( $M_A = 5.24$ ).

[11] In the first step, we choose three typical shock profiles at three different times within one shock self-reformation cycle, and we analyze separately the corresponding features

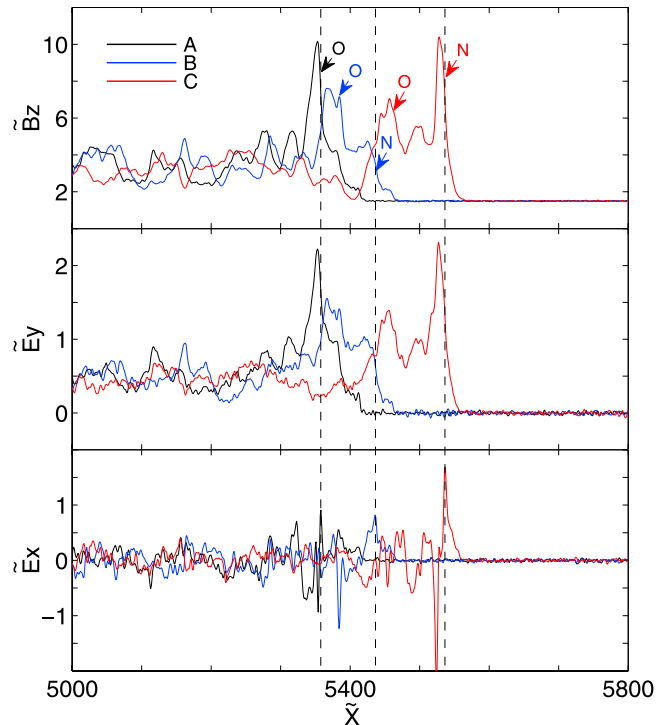


**Figure 2.** Plots of the shock profiles at three typical times. “O” and “N” denote the positions of the old and new ramps during one reforming cycle, respectively. (line A,  $\tilde{t} = 1552$ ; line B,  $\tilde{t} = 1600$ ; line C,  $\tilde{t} = 1744$ ). The main ramp location is marked by dashed line for each profile.

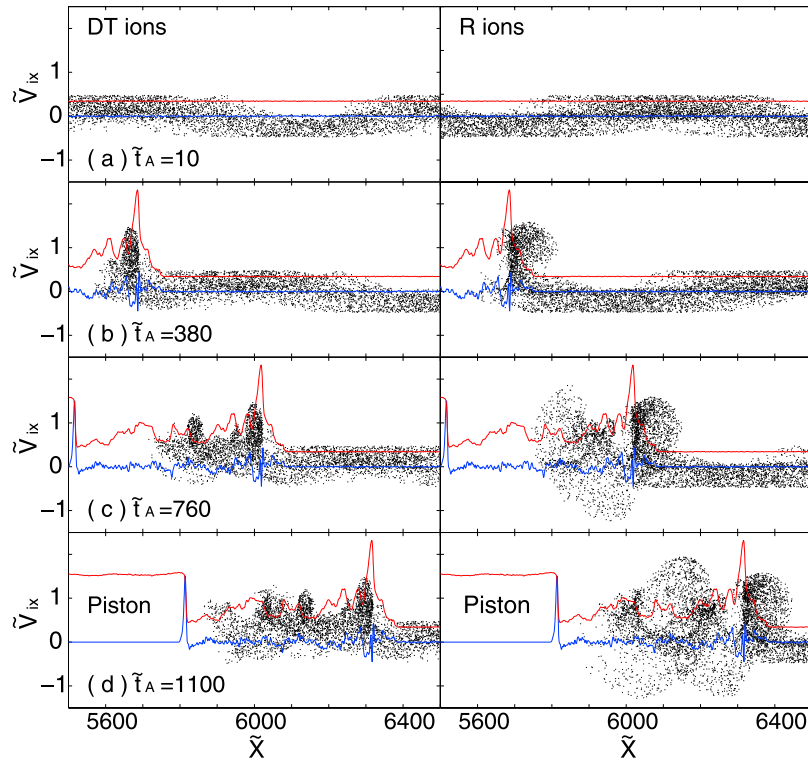


**Figure 3.** Evolution of phase space plots  $\tilde{v}_{ix}$  versus  $\tilde{x}_i$  (black dots) for (left) DT ions and (right) R ions at different times  $\tilde{t}_A$  of the test particle simulations performed with the shock profile A. The initial radius of the shell distribution is  $\tilde{V}_{shell} = 3.0\tilde{V}_A$ .  $\tilde{t}_A$  is measured from the time when profile A is chosen. The magnetic field  $\tilde{B}_z$  (red line) and electric field  $\tilde{E}_x$  (blue line) are also shown for reference. The magnetic piston in the downstream is also marked.

of ion acceleration. In a second step, we will analyze ion acceleration in a continuously evolving shock, and the shock is self-reforming when the test particles are moving. In both steps, we separate the upstream ions into two groups: the reflected (R) ions and directly transmitted (DT) ions, and describe their dynamics separately. The reflected ions have the following characteristics: after being reflected (1) their velocity in the  $x$  direction  $\tilde{v}_{ix}$  is larger than the shock propagating speed  $\tilde{V}_{shock}$ , and (2) they are located upstream the ramp  $\tilde{x}_i > \tilde{x}_{ramp}$ . Here the shock propagating speed is defined as the moving speed of the shock ramp. Furthermore, the R ions can be divided into two subpopulations by using a simple criteria in order to identify precisely some relevant information from a statistical analysis [Lever *et al.*, 2001]: the SDA ions are accelerated by the shock drift mechanism, and they are primarily reflected by the Lorenz force, i.e., in the ramp these verify  $\tilde{E}_x < \tilde{v}_{iy}\tilde{B}_z/\tilde{c}$ . SDA ions do return upstream once before passing through the shock front. The SSA ions are accelerated by the shock surfing acceleration, and they are primarily reflected by electrostatic force, i.e., in the ramp these verify  $\tilde{E}_x \geq \tilde{v}_{iy}\tilde{B}_z/\tilde{c}$ . In contrast with SDA process, SSA ions show multiple surfing reflections with a small normal amplitude as described by Lever *et al.* [2001]. It is important to remind that the trajectories of SDA and SSA ions only differ by the locations of their respective turning points around the ramp.

### 3.1. Fixed Shock Regime

[12] In this regime, three typical shock profiles (A, B and C) are selected from one self-reformation cycle (from  $\tilde{t} =$

1456 to 1744), and are shown in Figure 2. Profiles A, B and C represent the snapshots of  $\tilde{B}_z$ ,  $\tilde{E}_y$  and  $\tilde{E}_x$  at  $\tilde{t} = 1552$ , 1600 and 1744, respectively. In profile A, the shock front includes a ramp and a foot in front of the ramp, and the position of the ramp is denoted by “O”. In profile B, the amplitude of the old ramp “O” has decreased. Simultaneously, the foot amplitude increases and reaches a value at least equal to 50% of that of the ramp “O” and becomes a new ramp “N”. In profile C, the amplitude of the new ramp (“N”) has already overcome the old one (“O”). The ramps of profile A, B and C are respectively at  $\tilde{X} = 5359$ , 5436, and 5537, and their corresponding “instantaneous” propagating speeds along the  $x$  direction are  $5.47\tilde{V}_A$ ,  $6.25\tilde{V}_A$  and  $3.91\tilde{V}_A$ . Their corresponding widths of the shock front (include ramp and foot) are about  $\tilde{\delta}_{ramp} = 70$ , 98, and 42. For profiles B and C, the reference ramp used herein is the main “new” ramp (denoted by “N”), which has larger  $\tilde{E}_x$  than the other “old” ramp (denoted by “O”). The width of the shock front is measured from the beginning the foot to the maximum point of the magnetic overshoot [Walker *et al.*, 2004; Shimada and Hoshino, 2005], and the start of the foot is defined operationally as the location where the magnetic field has increased by 6.67% over its upstream value [Burgess *et al.*, 1989]. We will see that referring only the ramp is not enough and can be a source of misunderstanding, since the whole intricate shock front with which ions interact (being either reflected or directly transmitted) affects drastically the overall ion trajectories and their resulting energy gain.

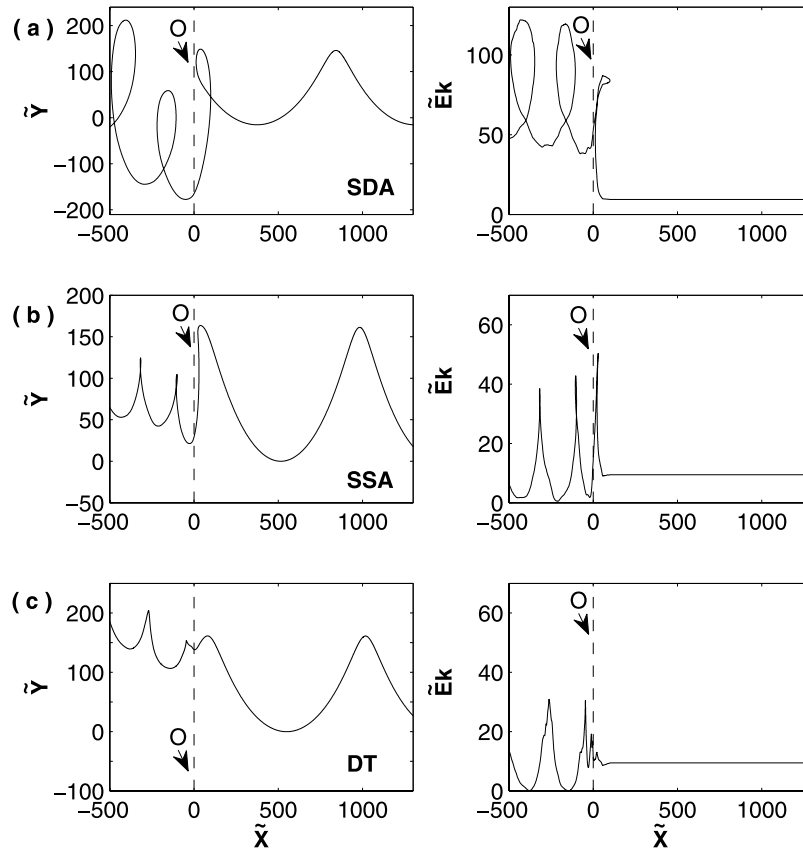


**Figure 4.** Three typical ion orbits and kinetic energy versus  $\tilde{X}$  obtained for shock profile A. (a) SDA, (b) SSA, and (c) DT ions. The shock ramp location is marked by dashed line “O”.

[13] Figure 3 shows the evolution of the ion phase space plots  $\tilde{v}_{ix}$  versus  $\tilde{x}_i$  for profile A, here the initial ion shell radius is  $\tilde{V}_{\text{shell}} = 3.0\tilde{V}_A$ . The magnetic field  $\tilde{B}_z$  and electric field  $\tilde{E}_x$  are also shown in Figure 3 for reference. When crossing the shock, the directly transmitted ions get a bulk velocity along the  $x$  direction primarily due to  $\tilde{E}_x \times \tilde{B}_z$  drift, and no noticeable heating can be found in the downstream. In contrast, reflected ions are accelerated to high energy during their reflections by the local electric field at the shock front and suffer an  $\tilde{E}_x \times \tilde{B}_z$  drift along the  $y$  direction (not shown here). Due to the gyromotion in the upstream magnetic field, they return to the shock front again and then succeed to transmit downstream. The dynamics of ions can be identified more clearly by tracing their trajectories. Figure 4 shows three typical ion trajectories which are traced in the shock rest frame, and the left column describes the ion trajectories while the right column shows their kinetic energy. At the ramp, SDA and SSA ions have much higher energy than DT ions, and the resulting energy gain is the highest for the SDA ion. In the downstream region, the resulting energy of SDA ion is much higher than that of SSA and DT ions.

[14] Figure 5 shows the domain in injection angle (gyrophase  $\phi$  and pitch angle  $\theta$ ) of the velocity space for the incident ions undergoing the SDA, SSA or DT process for profile A in different shell radii. Here the gyrophase  $\phi$  is defined as the angle between the  $+x$  direction (along the shock front normal) and the perpendicular component of the local ion velocity  $\tilde{v}_{i\perp}$  ( $\tilde{v}_{i\perp}$  denote the ion velocity perpen-

dicular to the ambient magnetic field), while the pitch angle  $\theta$  is the angle between the  $+z$  direction (along the ambient magnetic field) and the ion velocity vector. Both  $\phi$  and  $\theta$  are measured when the ion first reaches the beginning point of the foot. When the radius of the shell is smaller ( $0.5\tilde{V}_A$  in Figure 5a), the directly transmitted ions concentrate in two regions: in the first region  $\phi$  is around  $360^\circ$ , where the ions move along the  $+x$  direction; in the second region  $\theta$  is around  $0^\circ$  or  $180^\circ$ , where the ions move along the  $+z$  or  $-z$  direction. In the present case, these ions (their velocities are smaller than the shock propagating speed) are caught up with by the shock and then transmit the shock. The ions which are reflected by the shock front suffer shock drift acceleration only, and no SSA ions are evidenced. With the increase of the radius (Figure 5b), the domain of the directly transmitted ions expands from  $\phi$  around  $360^\circ$  to smaller values ( $190^\circ$ ). Simultaneously, the ions near the region where they move along the  $+x$  direction suffer shock surfing acceleration (SSA), since in this region  $\tilde{v}_y\tilde{B}_z/\tilde{c}$  is small and the electric force becomes more important. The larger the radius is (Figure 5c), the more particles are shock surfing accelerated but SSA process is mainly restricted to the domain  $\theta$  between  $45^\circ$  and  $135^\circ$ . Simultaneously, the domain of DT ions is expanding to a wide range ( $\phi$  between  $180^\circ$  and  $360^\circ$ ,  $\theta$  between  $0^\circ$  and  $180^\circ$ ). The reflected ions (both SSA and SDA) occupy the complementary domain. In general, the source of reflected ions is consistent with the results of previous papers [Burgess *et al.*, 1989; Lever *et al.*, 2001].

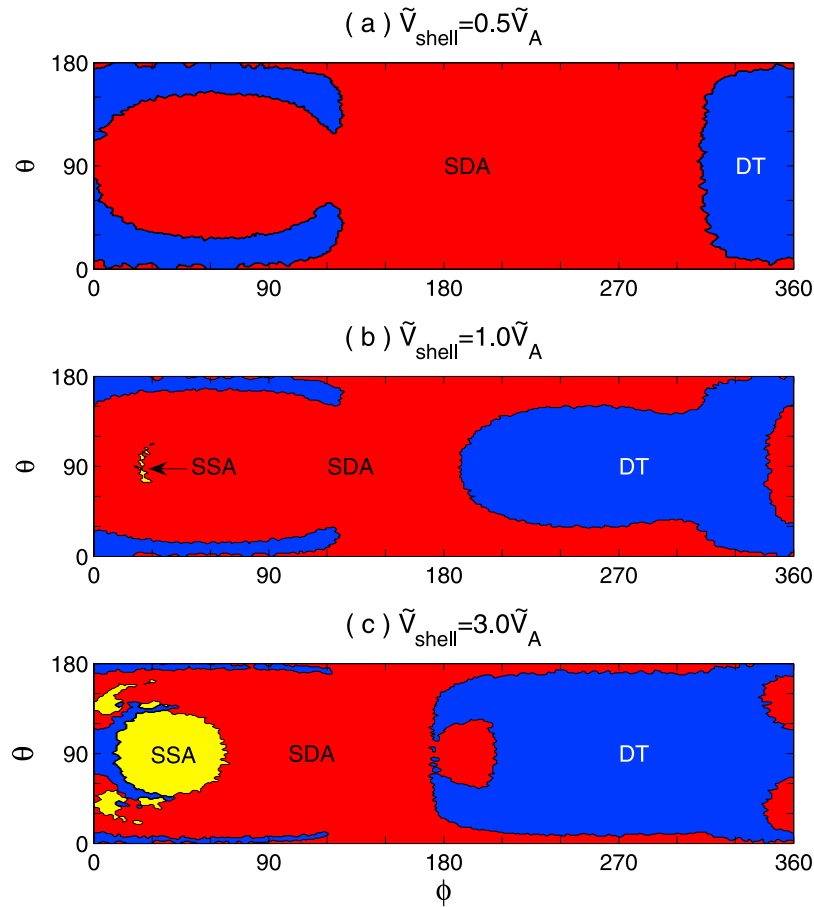


**Figure 5.** The angular domain in  $\phi$ - $\theta$  velocity space for the incident ions undergoing SDA (red), SSA (yellow), and DT (blue) at profile A. (a)  $\tilde{V}_{\text{shell}} = 0.5\tilde{V}_A$ . (b)  $\tilde{V}_{\text{shell}} = 1.0\tilde{V}_A$ . (c)  $\tilde{V}_{\text{shell}} = 3.0\tilde{V}_A$ .

[15] The behaviors of ions have also been investigated for profiles B and C. Figure 6 shows the ion phase space plots  $\tilde{v}_{ix}$  versus  $\tilde{x}_i$  and the domain in  $\phi - \theta$  space for the incident ions undergoing SDA, SSA or DT at profiles (a) B and (b) C, and the initial shell radius is  $3.0\tilde{V}_A$ . Here the SDA, SSA and DT particles are classified when the incident ions are interacted with the main shock ramp, which is the new shock ramp for both profile B and C (denoted by “N” in Figure 6). Most ions are directly transmitted through the shock front for profile B, while all ions are reflected for profile C. If we decrease the radius of the shell, all particles are directly transmitted through the shock front when the radius is sufficiently small (about  $2.0\tilde{V}_A$ ) for Profile B. For profile C, with the decrease of the shell radius, more particles suffer shock drift acceleration, and no directly transmitted ions are evidenced. Therefore, as the shock profile becomes steepy, the particles suffer more easily shock drift and surfing accelerations as in the case of profile C.

[16] Let us analyze more carefully the consequences of the shock front nonstationary (Figures 5c and 6) for a given shell radius ( $\tilde{V}_{\text{shell}} = 3\tilde{V}_A$ ). As the shock varies from profile A to B, the amplitude of the overshoot decreases and becomes very low (Figure 2) allowing a large percentage of incoming ions to pass through the shock front and to be directly transmitted. The foot amplitude increases but is not high enough to stop these particles. The width of the whole shock front including together the old ramp “O”, the foot

and the new ramp “N” is very broad. Most ions are directly transmitted whatever are their phase angles  $\theta$  and  $\phi$  (Figure 6a). Only a certain percentage of ions is reflected by the new ramp “N” and suffers SDA acceleration (Figure 6a). As the shock evolves from profile B to C, a steepened ramp builds up from the upstream edge of the foot and the overshoot reaches the maximum amplitude. Then, the ions are more easily reflected and suffer SDA and SSA processes (Figure 6b, bottom).

[17] In fact, the structures of the shock front becomes more complicated from profile B to C since another ramp “O” persists behind the new main ramp “N” (Figure 2), and ion trajectories strongly differ from those for profile A described above. In Figure 7, the dynamics of three typical trajectories is analyzed versus time in the shock rest frame for the intricate profile C. The locations of the sampled ions are indicated in Figure 6b (bottom panel; triangle, cross, and circle hold, respectively for the selected ions in Figures 7a, 7b and 7c). The left column of Figure 7 describes the ions trajectories while the right column shows their kinetic energy. The dashed lines correspond to the locations of ramp “O” and “N”. In Figure 7a, the first particle suffers shock surfing along the ramp “N” at the first stage; and then suffers multiple bounces between the two ramps “O” and “N” until getting energy high enough to penetrate into the downstream region. The associated energy gain is quite high during the first stage (SSA process where  $\tilde{E}_k \sim 50$  around time  $t_1$ ), and still

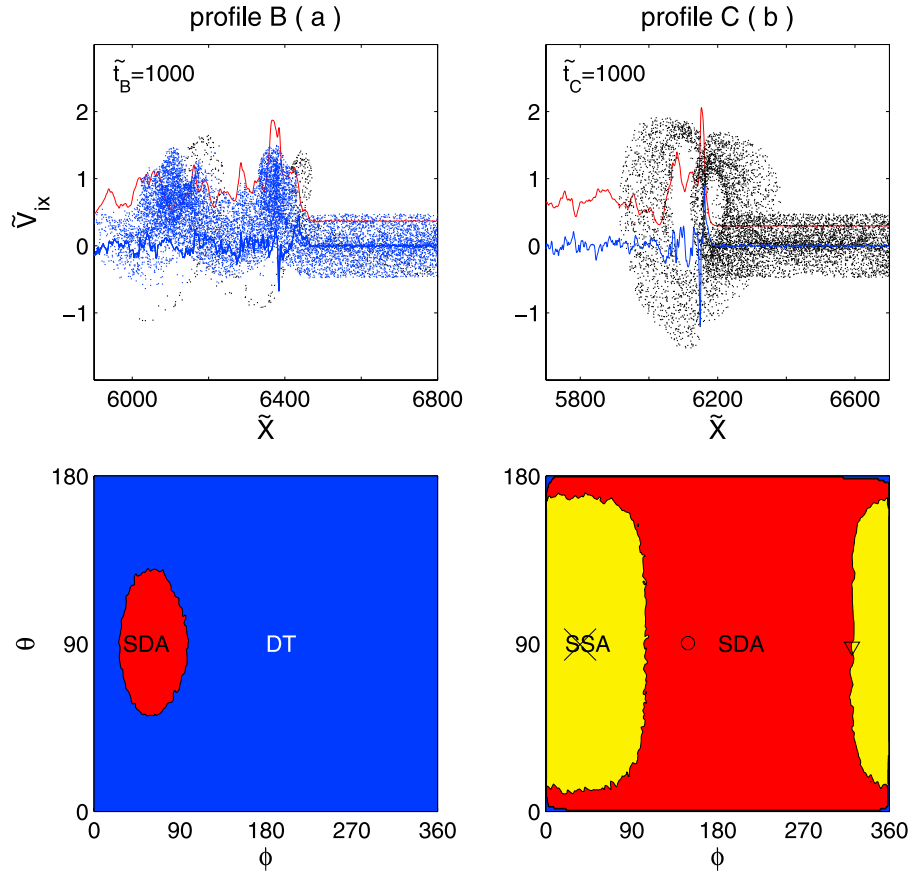


**Figure 6.** Phase space plots  $\tilde{v}_{ix}$  versus  $\tilde{x}_i$  for R (black dots) and DT (blue dots) ions, and the domain in  $\phi$ - $\theta$  velocity space (red, SDA; yellow, SSA; blue, DT) for incident ions with initial shell radius  $3.0\tilde{V}_A$  undergoing SDA, SSA, and DT for (a, left) profile B and (b, right) profile C. The magnetic field  $\tilde{B}_z$  (red line) and electric field  $\tilde{E}_x$  (blue line) are shown in the phase space plots for reference.

increases to reach its maximum ( $\sim 100$ ) between the two ramps (multiple bounces). In Figure 7b, the second particle first suffers shock surfing process along the main ramp “N”. Then, it undergoes a surfing process behind the main ramp (more exactly within the overshoot) until it acquires sufficiently high energy to break the potential barrier and to return upstream. One characteristic feature is that it returns upstream without reaching the old ramp “O”, which illustrates the impact of the large field fluctuations (in particular of the electrostatic field) between the two ramps on the ion dynamics. At last, the ion experiences an important shock drift with a very large gyroradius, and then it is accelerated to sufficiently high energy to be transmitted downstream (passing through both ramps “O” and “N”). This large drift (SDA) allows the ion to get a very large energy gain which is maximum between the two ramps locations (after time  $t_2$ ). In Figure 7c, the third particle suffers shock drift process at first stage (with respect to the location of the ramp “N”), but suffers a shock surfing almost immediately behind the new ramp and returns upstream. This SSA process within the overshoot is extremely efficient and the resulting energy gain is very large ( $\tilde{E}_k \sim 100$  at time  $t_1$ ). This process reveals to be much more efficient than that due to multiple bounces (as evidenced for the first particle). The efficiency can be explained as the ion suffers the effect of both large electro-

static ( $\tilde{E}_x = -2$ ) and magnetic field ( $\tilde{B}_z = 8.0$ ) around the overshoot (Figure 2), i.e., just behind the ramp location. At the time of profile C, the shock amplitude at the overshoot is the maximum within the self-reformation cycle. At last, the ion undergoes an important shock drift acceleration with a very large gyroradius allowing it to gain enough energy to be transmitted downstream, and this last stage is similar to that of the second particle (center panel). The only difference is that the large gyroradius allows the reflected ions to return more deeply with the upstream region. Present results lead to the following points: the highest and the quickest energy gain is associated to the third particle as it suffers an SSA process within the overshoot, which plays the role of a catapult. When combined with SDA at later times, the ion can get an even larger energy gain as it starts gyrating in the area where the magnetic field is maximum.

[18] Figure 8 shows the normalized downstream average kinetic energy for SDA and SSA particles as a function of the shell radius (from 0.1 to  $3.0\tilde{V}_A$ ) at shock profiles (a) A, (b) B and (c) C. At profiles B and C, we define the ions as SDA or SSA as they interact with the main ramp “N” of the shock for the first time. For clarifying the comparison, we calculate the average kinetic energy of the particles, whose positions are between  $\tilde{x}_{\text{ramp}} - 500 < \tilde{x}_i < \tilde{x}_{\text{ramp}} - 100$  at  $\tilde{t}_A = 1200$ ,  $\tilde{t}_B = 1100$  and  $\tilde{t}_C = 3000$  for profiles A, B and C,

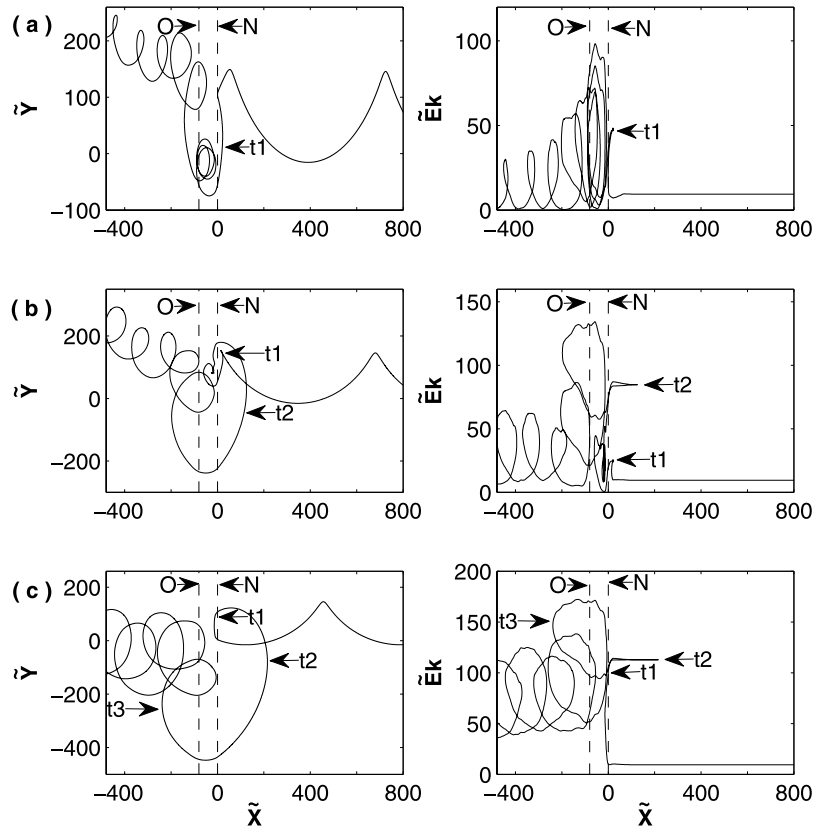


**Figure 7.** Three typical ion orbits and kinetic energy versus  $\tilde{X}$  obtained for shock profile C. Ions suffer from multistage accelerations. Dashed lines “O” and “N” denote the locations of the old and new ramps, respectively.

respectively. Present results show that the average kinetic energy of the SDA ions is proportional to their initial energy for all three profiles. For profile A, the average kinetic energy of the SSA ions is almost independent on their initial energy, which is consistent with the theory of shock surfing acceleration. For profile B, there is no SSA particles, and a few SDA ions appear for  $\tilde{V}_{\text{shell}}$  above a certain high values ( $2.3\tilde{V}_A$ ). For profile C, the average kinetic energy of the SSA now increases with their initial energy, since the so-called SSA ions suffer multistage accelerations within the complicated shock structure. As a consequence, the theory of shock surfing alone based on a simple shock profile (including mainly a ramp) cannot apply.

[19] In summary, the nonstationarity of the shock front has a strong impact on incoming ions: (1) the relative distribution of R and DT ions is strongly affected and varies between two extreme situations: almost no reflection (no transmission) and vice versa as the overshoot amplitude is very low (high) respectively; (2) the width of the whole shock front needs to be taken into consideration (not only the ramp) to investigate ion acceleration; (3) SSA and SDA processes are efficient as the ion shell radius  $\tilde{V}_{\text{shell}}$  is above a certain threshold but this threshold varies according to the instantaneous shock profile, which interacts with incoming ions, and (4) in the different shock profiles, SDA process reveals to be more efficient than SSA process to get a large

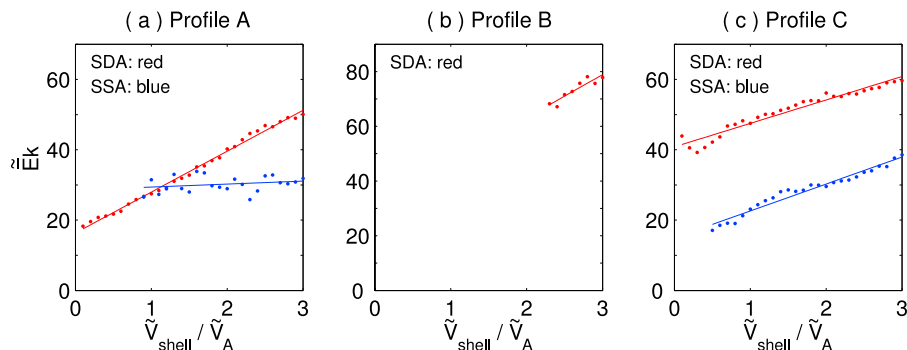


**Figure 8.** The average kinetic energy of SDA (red) and SSA (blue) in downstream as a function of their initial radius of the shell distribution at shock profiles (a) A, (b) B, and (c) C.

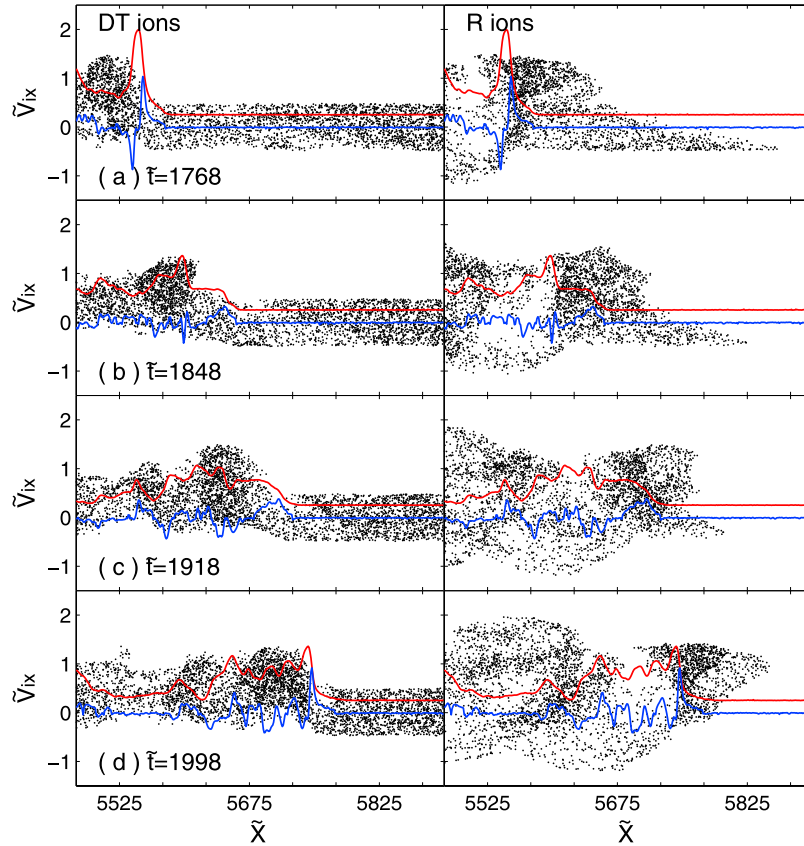


**Figure 9.** Evolution of phase space plots  $\tilde{v}_{ix}$  versus  $\tilde{x}_i$  for (left) DT and (right) R ions for the time-reforming shock regime. The initial radius of the shell distribution is  $3.0\tilde{V}_A$ . The magnetic field  $\tilde{B}_z$  (red line) and electric field  $\tilde{E}_x$  (blue line) are shown in the plots for reference.

average ion kinetic energy whatever  $\tilde{V}_{\text{shell}}$  is, and this gain is higher for larger  $\tilde{V}_{\text{shell}}$ .

### 3.2. Reforming Shock Regime

[20] In this regime, we investigate particle acceleration when the shock is nonstationary as shown in Figure 1. Test particles are also distributed evenly within a wide region  $100 < \tilde{x}_i - \tilde{x}_{\text{ramp}} < 1420$  at a chosen starting time  $\tilde{t} = 628$ . Then all particles have enough time to interact with the propagating shock over at least one full self-reformation cycle. Figure 9 shows the evolution of ion phase space plots  $\tilde{v}_{ix}$  versus  $\tilde{x}_i$  at different times, and the initial radius of the shell distribution is  $\tilde{V}_{\text{shell}} = 3.0\tilde{V}_A$ . As in the fixed shock regime, the reflected ions can be accelerated to high energy by the shock front, and the number of the reflected ions varies with time due to the nonstationarity of the shock, which is in a good agreement with previous results of *Lembege and Savoini [1992]*.

[21] The ion dynamics can be identified more clearly by tracing their trajectories, and Figure 10 shows four typical ion trajectories. In Figure 10, the left column describes the ion trajectories, and the right column shows their kinetic energy. In Figure 10a, the ion first undergoes SSA from A1 to B1 since  $\tilde{E}_x > \tilde{v}_{iy}\tilde{B}_z/\tilde{c}$  at the reflected point A1. Then, the ion interacts with the new ramp of the shock at B1 where it is accelerated to higher energy and then transmits to downstream. In Figure 10b, the ion first suffers SDA process A2 to C2 due to  $\tilde{E}_x < \tilde{v}_{iy}\tilde{B}_z/\tilde{c}$  at the reflected point

B2. The ion interacts with the new ramp of the shock at C2 and succeeds to be transmitted. Figure 10c describes an ion multistage acceleration. From A3 to C3 the ion first suffers an SDA acceleration since  $\tilde{E}_x < \tilde{v}_{iy}\tilde{B}_z/\tilde{c}$  at the reflected point B3. It hits the ramp at a time between A3 and B3 when the overshoot is the highest (indicated by the yellow line) and then describes a large Larmor orbit upstream. At last, it interacts again with the shock front around C3 and goes downstream. Figure 10d shows an ion which directly transmits into the downstream, and no obvious acceleration is found. In general, the ions can be accelerated to high energy with SSA, SDA or multistage acceleration. These various results confirm again (1) the strong impact of the shock front nonstationarity on the resulting ion dynamics; (2) that initial SDA process seems to provide the highest resulting energy gain; (3) the necessity to include the overall width of the varying shock front for analyzing the resulting ion dynamics (and not only the ramp).

[22] Figure 11 shows the domain in injection angle (gyrophase  $\phi$  and pitch angle  $\theta$ ) of the velocity space for the incident ions undergoing SDA, SSA or DT processes. Since some ions undergo multistage acceleration, we identify the type of ion acceleration when ions interact with the main shock ramp for the first time. The situation is much more complicated than that of the fixed shock profile. With the increase of the radius, more particles are accelerated with SSA mechanism, while the SDA mechanism plays an important role for ions with both lower and higher initial

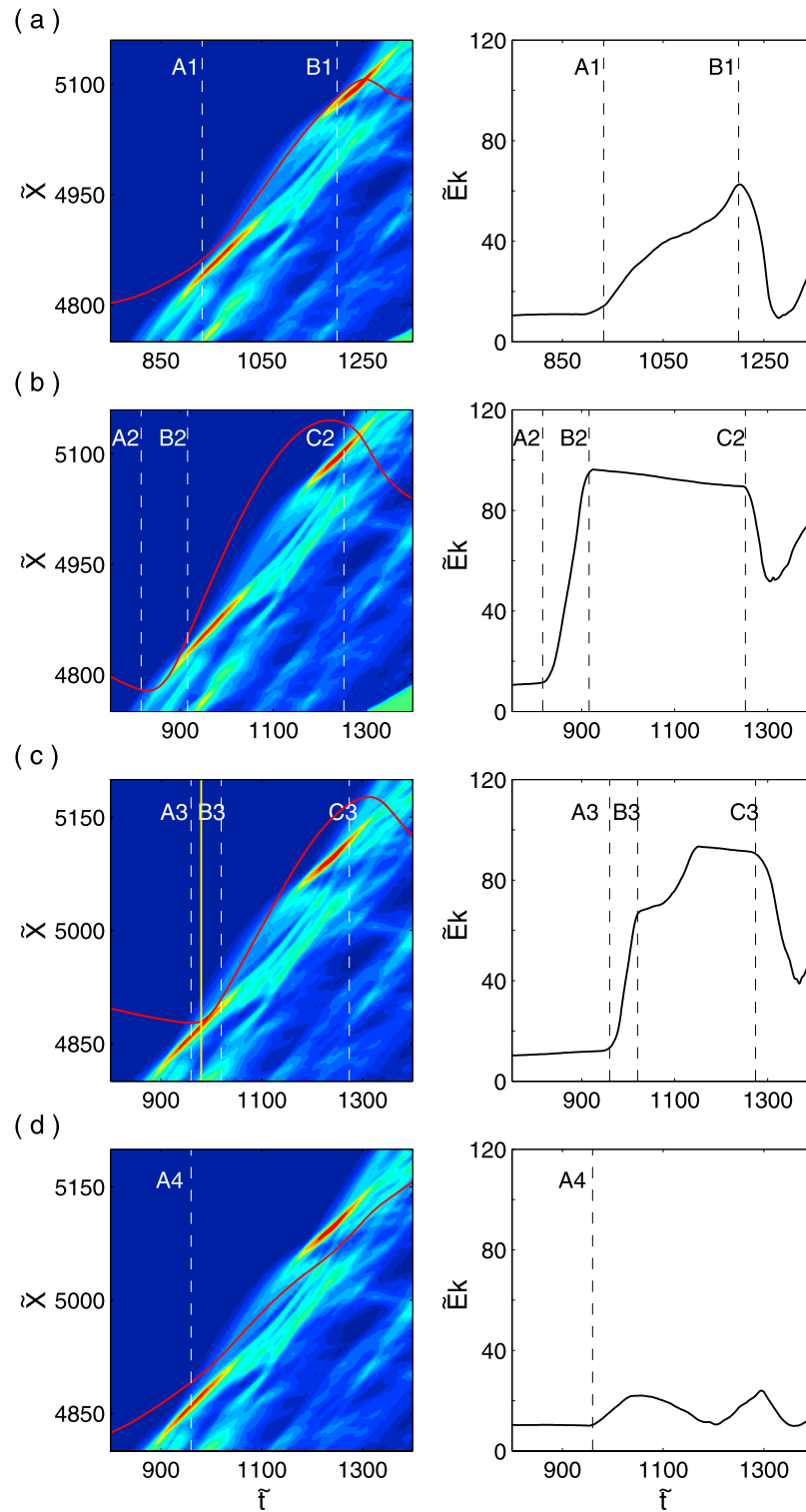


**Figure 10.** Four typical (left) ion trajectories and (right) kinetic energy versus time for the time-reforming shock regime. The vertical dash lines denote some key points.

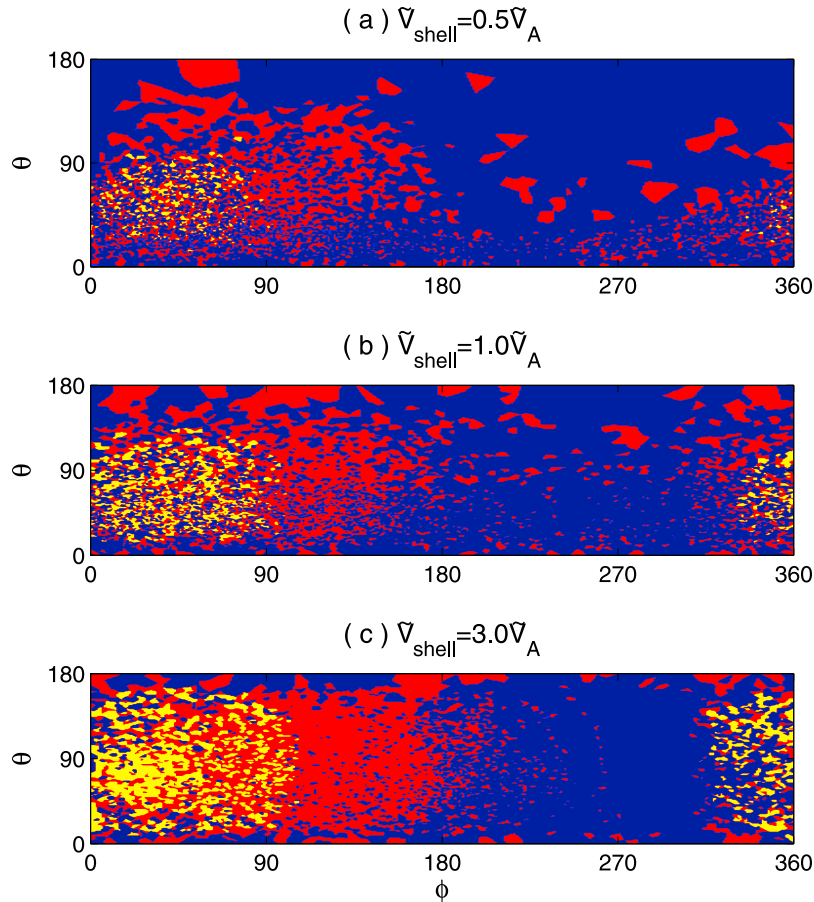


**Figure 11.** Angular domain in  $\phi$ - $\theta$  velocity space for SDA (red), SSA (yellow), and DT (blue) ions for (a)  $\tilde{V}_{\text{shell}} = 0.5\tilde{V}_A$ , (b)  $\tilde{V}_{\text{shell}} = 1.0\tilde{V}_A$ , and (c)  $\tilde{V}_{\text{shell}} = 3.0\tilde{V}_A$ . Results are obtained for the time-reforming shock regime.

energy. The DT, SSA and SDA ions tend to concentrate in the region where  $\phi$  is around  $270^\circ$ ,  $45^\circ$  and  $135^\circ$ , respectively. Different from the results in the fixed shock profile, the regions of the SDA, SSA or DT ions are now more clearly separated due to the nonstationarity of the shock front.

[23] Figure 12 shows (a) the downstream average kinetic energy and (b) the percentage of the SDA, SSA and DT particles as a function of the shell radius. These quan-

ties are calculated when their locations are between  $\tilde{x}_{\text{ramp}} - 500 < \tilde{x}_i < \tilde{x}_{\text{ramp}} - 100$  at  $\tilde{t} = 2064$ . For the SDA ions, the average kinetic energy approximately increases linearly with the initial energy; their percentage first decreases and then increases slowly  $\tilde{V}_{\text{shell}} > 1.2\tilde{V}_A$ . For the SSA ions, the average kinetic energy increases smoothly with the initial energy; their percentage first increases and then stays almost constant  $\tilde{V}_{\text{shell}} > 1.2\tilde{V}_A$ . The increase of the kinetic energy for

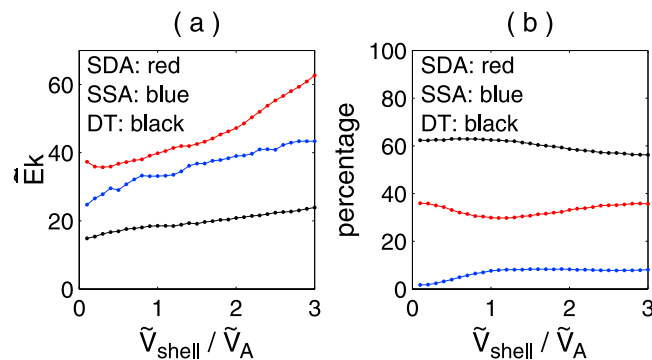


**Figure 12.** (a) The average kinetic energy of SDA (red), SSA (blue), and DT (black) ions in downstream and (b) their percentage as a function of their initial radius of the shell distribution. Results are obtained for the time-reforming shock regime.

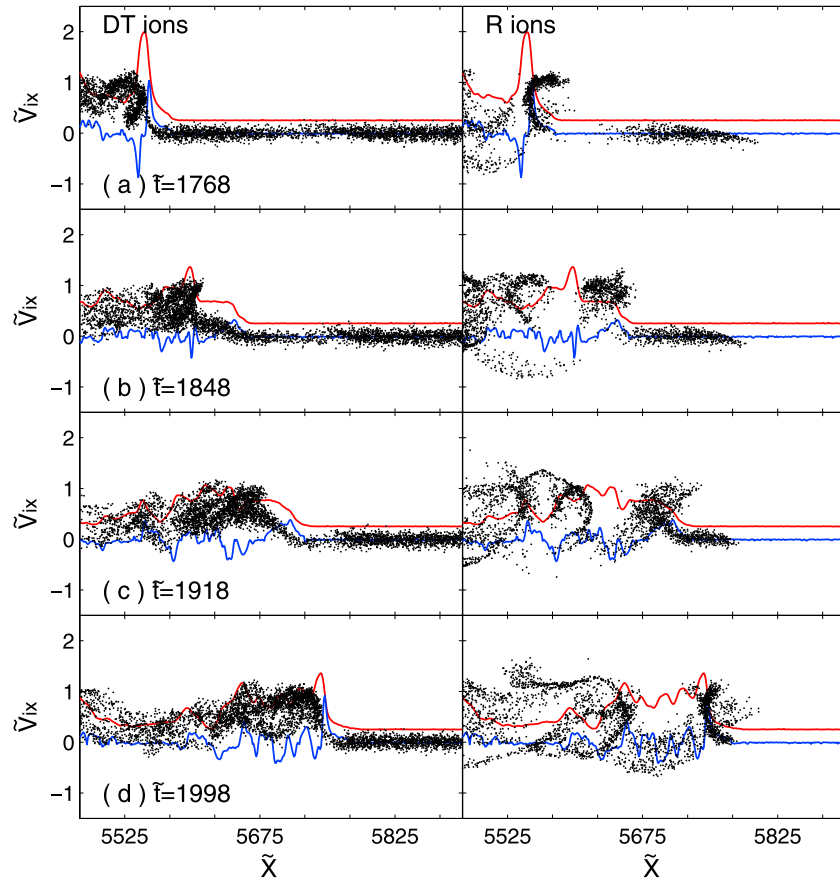


**Figure 13.** Evolution of phase space plots  $\tilde{v}_{ix}$  versus  $\tilde{x}_i$  for (left) DT ions and (right) R ions, and here, the ions have Maxwellian distribution with the initial thermal speed  $0.5\tilde{V}_A$ . The magnetic field  $\tilde{B}_z$  (red line) and electric field  $\tilde{E}_x$  (blue line) are shown in the plots for reference. Results are obtained for the time-reforming shock regime.

SSA (and of SDA) ions is certainly due to the multi-stage acceleration that these ions suffer with the complicated self-reforming shock front, and no simple relation can be established.

[24] Figure 13 shows the evolution of ion phase space plots  $\tilde{v}_{ix}$  versus  $\tilde{x}_i$  at different times. Initially, the ion velocity distribution is Maxwellian with the thermal speed  $\tilde{V}_t = 0.5\tilde{V}_A$ . The Maxwellian distribution can be considered as a weighted superposition of a series of shell distributions. Similar to Figure 9, the number of the reflected ions varies with time due to the nonstationarity of the shock front. This can be seen more clearly in Figure 14, which describes the time evolution of the maximum values of (a)  $\tilde{E}_x$  and (b)  $\tilde{B}_z$  between  $\tilde{x}_{\text{ramp}} - 20$  and  $\tilde{x}_{\text{ramp}} + 20$ , and the percentage of the reflected ions in the region  $\tilde{x}_{\text{ramp}} < \tilde{x}_i < 2L_x$  for (c) the shell distributions and (d) Maxwellian distributions. Obviously, the cyclic period of the reflected ions percentage is equal to that of the shock front self-reformation. With the increase of the initial energy, the effects of the shock nonstationarity gradually decreases. These results show that the variation of the reflected ions percentage is stronger for small shell radius or thermal velocity (Maxwellian distribution). These results are in agreement with previous works, where the self-reformation is strongly associated with the variation of reflected ions percentage when  $\beta_i$  is

quite weak [Lembege and Savoini, 1992] or equivalent the ratio  $\tilde{V}_{\text{shock}}/\tilde{V}_{\text{thi}}$  is quite large [Scholer et al., 2003].

#### 4. Conclusions and Discussions

[25] Previous particle-in-cell simulations have already evidenced that quasiperpendicular shocks are nonstationary and can self-reform on gyro scale of the incoming ions [Biskamp and Welter, 1972; Lembege and Dawson, 1987; Scholer et al., 2003]. In this paper, we separate the incoming ions into reflected and directly transmitted parts during their interaction with the shock front, and then investigate the mechanisms of ion acceleration in nonstationary perpendicular shock. Most energetic particles correspond to the reflected ions which are accelerated by SSA and SDA mechanisms. The ion dynamics depends largely on the structures of the shock with which incoming ions interact. Therefore as the shock evolves with time, the number of the reflected ions and the resulting energy gain strongly vary, the dynamics of particles is more complicated than in fixed shock profile.

[26] The above conclusions are obtained by using test particles with shell velocity distributions of different radii. This simple approach is helpful before considering more realistic Maxwellian distributions, because Maxwellian dis-

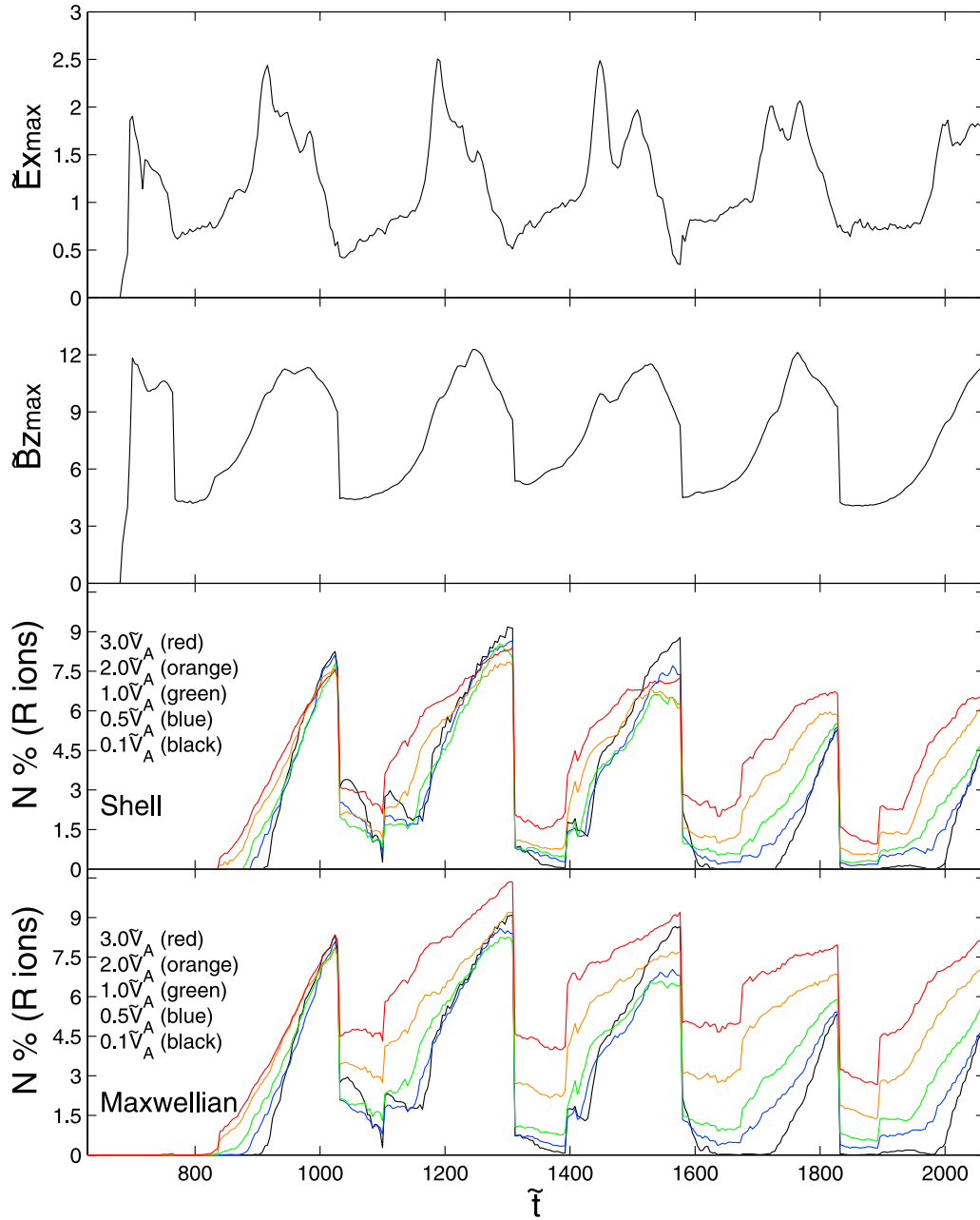


**Figure 14.** Time history of the maximum values of the electrostatic field  $\tilde{E}_{x \max}$  and the magnetic field  $\tilde{B}_{z \max}$  around the shock ramp and of the number of the reflected ions. Results are obtained for different radii (shell distribution) and thermal velocity (Maxwellian distribution), respectively.

tribution is a weighted superposition of a series of shell velocity distributions with different radii. In extension to the previous results of hybrid simulations [Burgess *et al.*, 1989], we also find (1) whether a given ion is accelerated primarily depends on the time at which ions interact with the shock front, and (2) energetic particles (SSA and SDA reflected ions) come from a limited portion of the incident distribution, rather than being randomly selected. However, in the hybrid simulations, where the structure of the shock profile is fixed, none of the reflected ions comes from the core of Maxwellian distribution. In contrast, we find that for the nonstationary shocks, the reflected ions not only come from the wings of the Maxwellian distribution (equivalent to large radius of the shell velocity distribu-

tion), but also from the core of the Maxwellian distribution (equivalent to small radius of the shell velocity distribution). The varying structures of the shock front have a strong impact on ion reflection. The whole shock front and not only the ramp needs to be included to investigate ion acceleration.

[27] In the diffusive shock acceleration (DSA) process, particles suffer multiple bounces back and forth when interacting with some turbulent shock profile. In this process, the particles can be accelerated to very high energy. Such profiles are common in quasiparallel shock. This DSA process requires a certain threshold be reached (by some preacceleration) in order to be efficient, especially for quasiperpendicular shock. Moreover, the acceleration mech-

anisms of reflected ions by nonstationary shocks discussed in this paper might be possible candidates for preacceleration that can initiate the DSA mechanism in quasiperpendicular shocks, and accelerate ions to even higher energy. Although we only discuss shock acceleration in perpendicular shocks, the conclusions should be extended to quasiperpendicular shocks. This extensive work is under active investigation.

[28] **Acknowledgments.** This research was supported by the National Science Foundation of China grants 40725013, 40674093, 40574063, and Chinese Academy of Sciences KJXC2-YW-N28. The initial one-dimensional PIC simulations have been performed on the supercomputer of IDRIS center located at Orsay (near Paris).

[29] Amitava Bhattacharjee thanks Nobue Shimada and another reviewer for their assistance in evaluating this paper.

## References

- Axford, W. I., E. Lee, and G. Skadron (1977), The acceleration of cosmic rays by shock waves, *Proc. Int. Conf. Cosmic Rays 15th*, 11, 132.
- Bell, A. R. (1978a), The acceleration of cosmic rays in shock front: I, *Mon. Not. R. Astrophys. Soc.*, 182, 147–156.
- Bell, A. R. (1978b), The acceleration of cosmic rays in shock front: II, *Mon. Not. R. Astrophys. Soc.*, 182, 443–455.
- Begelman, M., and J. G. Kirk (1990), Shock-drift particle acceleration in superluminal shocks: A model for hot spots in extragalactic radio sources, *Astrophys. J.*, 353, 66–80.
- Biskamp, D., and H. Welter (1972), Ion heating in high-Mach-number, oblique, collisionless shock waves, *Phys. Rev. Lett.*, 28, 410–413.
- Blandford, R., and D. Eichler (1987), Particle acceleration at astrophysical shocks: A theory of cosmic ray origin, *Phys. Rep.*, 154, L1–L75.
- Blandford, R. D., and J. P. Ostriker (1978), Particle acceleration by astrophysical shocks, *Astrophys. J.*, 221, L29–L32.
- Burgess, D. (1995), *Introduction to Space Physics*, edited by M. G. Kivelson and C. T. Russell, pp. 129–155, Cambridge Univ. Press, Los Angeles, Calif.
- Burgess, D., W. P. Wilkinson, and S. J. Schwartz (1989), Ion distributions and thermalization at perpendicular and quasi-perpendicular supercritical collisionless shocks, *J. Geophys. Res.*, 94, 8783–8792.
- Chalov, S. V. (2001), Shock drift acceleration of pickup protons at corotating interaction regions, *J. Geophys. Res.*, 106, 18,667–18,675.
- Decker, R. B. (1988), Computer modeling of test particle acceleration at oblique shocks, *Space Sci. Rev.*, 48, 195–262.
- Decker, R. B., and L. Vlahos (1985), Shock drift acceleration in the presence of waves, *J. Geophys. Res.*, 90, 47–56.
- Giacalone, J. (2004), Large-scale hybrid simulations of particle acceleration at a parallel shock, *Astrophys. J.*, 609, 452–458.
- Hada, T., M. Oonishi, B. Lembege, and P. Savoini (2003), Shock front nonstationarity of supercritical perpendicular shocks, *J. Geophys. Res.*, 108(A6), 1233, doi:10.1029/2002JA009339.
- Hellinger, P., P. Trávníček, and H. Matsumoto (2002), Reformation of perpendicular shocks: Hybrid simulations, *Geophys. Res. Lett.*, 29(24), 2234, doi:10.1029/2002GL015915.
- Hudson, P. D. (1965), Reflection of charged particles by plasma shocks, *Mon. Not. R. Astron. Soc.*, 131, 23.
- Katsouleas, T., and J. M. Dawson (1983), Unlimited electron acceleration in laser-driven plasma waves, *Phys. Rev. Lett.*, 51, 392–395.
- Lee, M. A. (1983), Coupled hydromagnetic wave excitation and ion acceleration at interplanetary traveling shocks, *J. Geophys. Res.*, 88, 6109–6119.
- Lee, M. A. (1999), The injection, acceleration, and dynamical influence of interstellar pickup ions at the solar wind termination shock, *Astrophys. Space Sci.*, 264, 497–508.
- Lee, M. A., V. D. Shapiro, and R. Z. Sagdeev (1996), Pickup ion energization by shock surfing, *J. Geophys. Res.*, 101, 4777–4789.
- Lee, R. E., S. C. Chapman, and R. O. Dendy (2004), Numerical simulations of local shock reformation and ion acceleration in supernova remnants, *Astrophys. J.*, 604, 187–195.
- Lee, R. E., S. C. Chapman, and R. O. Dendy (2005), Ion acceleration processes at reforming collisionless shocks, *Phys. Plasmas*, 12, 012901.
- Lembege, B., and J. M. Dawson (1987), Self-consistent study of a perpendicular collisionless and nonresistive shock, *Phys. Fluids*, 30, 1767–1788.
- Lembege, B., and P. Savoini (1992), Nonstationarity of a two-dimensional quasiperpendicular supercritical collisionless shock by self-reformation, *Phys. Fluids*, B4, 3533–3548.
- Lever, E. L., K. B. Quest, and V. D. Shapiro (2001), Shock surfing vs. shock drift acceleration, *Geophys. Res. Lett.*, 28, 1367–1370.
- Li, G., G. P. Zank, and W. K. M. Rice (2003), Energetic particle acceleration and transport at coronal mass ejection drive shocks, *J. Geophys. Res.*, 108(A2), 1082, doi:10.1029/2002JA009666.
- Lipatov, A. S., and G. P. Zank (1999), Pickup ion acceleration at low- $\beta_p$  perpendicular shocks, *Phys. Rev. Lett.*, 82, 3609–3612.
- Lipatov, A. S., G. P. Zank, and H. L. Pauls (1998), The acceleration of pickup ions at shock waves: Test particle-mesh simulations, *J. Geophys. Res.*, 103, 29,679–29,696.
- Malkov, M. A., and L. O’C. Drury (2001), Nonlinear theory of diffusive acceleration of particles by shock waves, *Rep. Prog. Phys.*, 64, 429–481.
- Nishimura, K., H. Matsumoto, H. Kojima, and S. Gary (2003), Particle simulation of re-formation at collisionless perpendicular shocks: Coherent behavior of reflected ions, *J. Geophys. Res.*, 108(A5), 1182, doi:10.1029/2002JA009671.
- Sagdeev, R. Z. (1966), Cooperative phenomena and shock waves in collisionless plasmas, *Rev. Plasma Phys.*, 4, 23–91.
- Schmitz, H., S. C. Chapman, and R. O. Dendy (2002), Electron preacceleration mechanisms in the foot region of high Alfvén Mach number shocks, *Astrophys. J.*, 579, 327–336.
- Scholer, M., and S. Matsukiyo (2004), Nonstationarity of quasiperpendicular shocks: A comparison of full particle simulations with different ion to electron mass ratio, *Ann. Geophys.*, 22, 2345–2353.
- Scholer, M., I. Shinohara, and S. Matsukiyo (2003), Quasi-perpendicular shocks: Length scale of the cross-shock potential shock reformation, and implication for shock surfing, *J. Geophys. Res.*, 108(A1), 1014, doi:10.1029/2002JA009515.
- Shapiro, V. D., and D. Ucer (2003), Shock surfing acceleration, *Planet. Space Sci.*, 51, 665–680.
- Shimada, N., and M. Hoshino (2000), Strong electron acceleration at high Mach number shock waves: Simulation study of electron dynamics, *Astrophys. J.*, 543, L67–L71.
- Shimada, N., and M. Hoshino (2005), Effect of strong thermalization on shock dynamical behavior, *J. Geophys. Res.*, 110, A02105, doi:10.1029/2004JA010596.
- Tsubouchi, K., and B. Lembege (2004), Full particle simulations of short large-amplitude magnetic structures (SLAMS) in quasi-parallel shocks, *J. Geophys. Res.*, 109, A02114, doi:10.1029/2003JA010014.
- Ucer, D., and V. D. Shapiro (2001), Unlimited relativistic shock surfing acceleration, *Phys. Rev. Lett.*, 87, 075001.
- Ucer, D., and V. D. Shapiro (2005), Relativistic surfing acceleration of ions at oblique shocks, *Phys. Lett. A*, 346, 163–167.
- Walker, S. N., H. St. C. K. Alleyne, M. A. Balikhin, M. Andre, and T. S. Horbury (2004), Electric field scales at quasi-perpendicular shocks, *Ann. Geophys.*, 22, 2291–2300.
- Webb, G. M., W. I. Axford, and T. Terasawa (1983), On the drift mechanism for energetic charged particles at shocks, *Astrophys. J.*, 270, 537–553.
- Webb, G. M., G. P. Zank, M. Ko, and D. J. Donohue (1995), Multidimensional Green’s functions and the statistics of diffusive shock acceleration, *Astrophys. J.*, 453, 178–206.
- Zank, G. P., H. L. Pauls, I. H. Cairns, and G. M. Webb (1996), Interstellar pickup ions and quasi-perpendicular shocks: Implications for the termination shock and interplanetary shocks, *J. Geophys. Res.*, 101, 457–477.
- Zank, G. P., G. Li, V. Florinski, Q. Hu, D. Lario, and C. W. Smith (2006), Particle acceleration at perpendicular shock waves: Model and observations, *J. Geophys. Res.*, 111, A06108, doi:10.1029/2005JA011524.

B. Lembège, Centre d’étude des Environnements Terrestre et Planétaires, CNRS Université de Versailles-Saint Quentin, 10-12 Avenue de l’Europe, F-78140 Velizy, France. (bertrand.lembege@cetp.ipsl.fr)

Q. M. Lu, S. Wang, and Z. W. Yang, School of Earth and Space Sciences, University of Science and Technology of China, 96 Jin Zhai Road, Hefei, Anhui 230026, China. (qmlu@ustc.edu.cn; swan@ustc.edu.cn; zwyang@mail.ustc.edu.cn)